Advancing 4D Printing Through Designing Interlocking Blocks: Enhancing Deformation Uniformity in Active Composite Structures

Kheira Benyahia[1], Hichem Seriket[1], Sébastien Blanquer[2], Samuel Gomes[1], Mahdi Bodaghi[3], Jean-Claude André[4], Kun Zhou[5], H. Jerry Qi[6], Frédéric Demoly[1,7] *

[1]ICB UMR 6303 CNRS, Belfort-Montbeliard University of Technology, UTBM, 90010 Belfort, France
[2]ICGM, University of Montpellier, CNRS, ENSCM, Montpellier 34000, France
[3]Department of Engineering, School of Science and Technology, Nottingham Trent University, Nottingham NG11 8NS, UK
[4]LRGP 7274 UMR CNRS, University of Lorraine, Nancy, France
[5]Singapore Centre for 3D Printing, School of Mechanical and Aerospace Engineering, Nanyang Technological University, 50 Nanyang Avenue, Singapore 639798, Singapore
[6]The George W. Woodruff School of Mechanical Engineering, Georgia Institute of Technology, Atlanta, GA 30332, USA
[7]Institut universitaire de France (IUF)
*Corresponding author: Frédéric Demoly, frederic.demoly@utbm.fr

Abstract

Interlocking assemblies have been explored to address large assembly and complex parts and are now integral to additive manufacturing (AM) for creating objects with dissimilar materials and multiple properties. 4D printing technology, which combines smart materials (SMs) with AM, aligns with this approach by enabling the creation of objects that can change shape or properties when exposed to external stimuli. As 4D printing trends towards strategically arranging active and passive materials for improved control and performance, challenges arise due to the limited compatibility of existing 3D printers with the required SM properties. To address this issue, interlocking blocks of dissimilar materials can be printed and then assembled into a desired shape. This work aims to generalize the applicability of the interlocking block assembly approach. This will be achieved by improving the deformation uniformity in a 4D multi-material interlocked assembly. This paper also addresses limitations that can occur due to the interfaces between interlocking blocks, such as lack of deformation and contact continuity. Thus, it will be a question of customizing the shapes of the blocks in the early stages of assembly generation, considering SMs and their potential transformations. Finally, this approach is illustrated with an example, shedding light on the practical implications.

Keywords: 4D printing, interlocking blocks, shape change, active composite structures, deformation uniformity.

1. Introduction

This paper explores the synergistic relationship between multi-material 4D printing and the design of interlocking assembly blocks. In the context of this study, 4D printing refers to the additive

manufacturing (AM) process that involves the fabrication of objects using materials capable of undergoing controlled, programmable changes in shapes and properties over time in response to external stimuli. From a manufacturing standpoint, 4D printing is currently explored through both single-material and multi-material printing [1-5]. While both avenues require ongoing attention to advance scientific knowledge in 4D printing, multi-material 4D printing stands out for its ability to produce parts with specific shape and property change capacities while maintaining robust mechanical performance [6,7]. This manufacturing progress has brought about a shift in design approaches, providing newfound freedom in shaping and structuring smart devices with both hard and soft properties [3,6,8-10].

Despite these advancements, additional research efforts are crucial to overcome the remaining manufacturing and stimulation barriers. Key challenges include addressing the lack of AM process compatibility and the availability of smart materials (SMs), as well as comprehensive multi-material deposition capabilities. Another significant challenge is to effectively manage the energy consumption of stimulation to prevent low actuator efficiency [3,11-13]. A promising strategy to address these limitations involves utilizing interlocking mechanisms to assemble a multi-material 4D structure from a discrete set of interlocking parts made by different materials and printed using multiple AM techniques [6-7]. Beyond overcoming current limitations in 4D printing technology, the use of computational interlocking mechanisms holds great promise for expanding design freedom. Notably, Benyahia et al. [6,7] recently proposed a computational design approach based on interlocking block assembly dedicated to multi-material 4D printing (**Figure 1**). The essence of this approach lies in decomposing a 4D voxel-based model with a multi-material digital distribution into subassemblies of voxels, or blocks, reminiscent of polycubes in discrete geometry. These subassemblies are intended to be printed separately and then assembled [6,14-19].

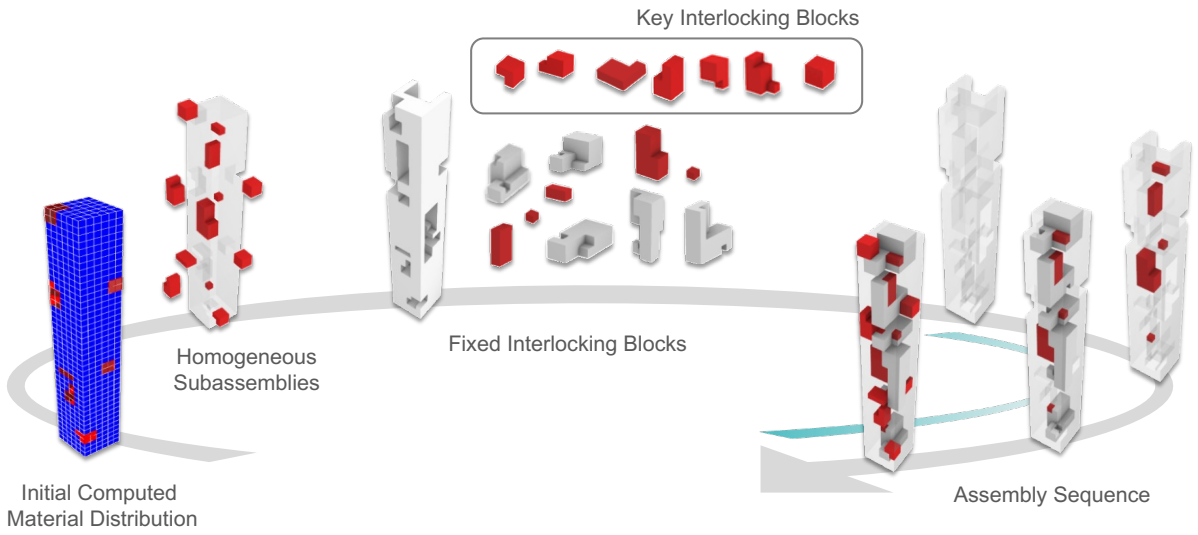

Figure 1. Computational design of complex material distribution into interlocking blocks for 4D printing.

Building upon this foundation, the main objective is to design interlocking assembly blocks to ensure contact continuity and deformation uniformity. For instance, customizing the shapes of the interlocking blocks grants the ability to perfectly suit specific utilization requirements and optimize their functionality and performance [20-22]. Another key advantage of utilizing the customized interlocking blocks is the simplification it brings to the assembly process [23,24]. By building customized blocks with specific shapes, the streamlining of the assembly workflow saves valuable time and effort by avoiding additional computation of the interlocking blocks. Additionally, such types of interlocking blocks offer the advantage of not only being recyclable but also versatile in their assembly [25-27]. The sustainability and versatility aspects of customized interlocking blocks align perfectly with the commitment to reducing waste and promoting environmentally friendly manufacturing practices. Furthermore, leveraging such a concept enables us to advance toward the automation of robot-guided assembly. This is due to the predefined and standard nature of the blocks. Incorporating robot-guided assembly techniques enables the achievement of higher levels of accuracy, repeatability, and efficiency in constructing interlocked structures. Moreover, the customization of interlocking blocks offers exciting possibilities for multi-scale interlocking assembly, as it allows for the control of voxel sizes [26]. It is to say that interconnected systems and structures at various levels of detail can be created, allowing for the development of complex and adaptable architectures.

In this study, the potential of the customized interlocking blocks will be harnessed from a different perspective. Building upon the algorithm developed in [6,7] interlocking blocks can be generated to construct 4D multi-material structures capable of undergoing shape/property transformations when stimulated, our proposed approach focuses on assigning specific block shapes to ensure deformation uniformity. Indeed, in some cases of shape transformations (**Figure 2a**), particularly when using certain SMs, the interfaces within the assembly may not keep up with the overall deformation of the structure. This is typically the case in active composite structures that combine inert and active materials with expansion/contraction function (e.g., swelling/deswelling hydrogels). This lack of contact and deformation continuity can impede the uniformity of the overall deformation.

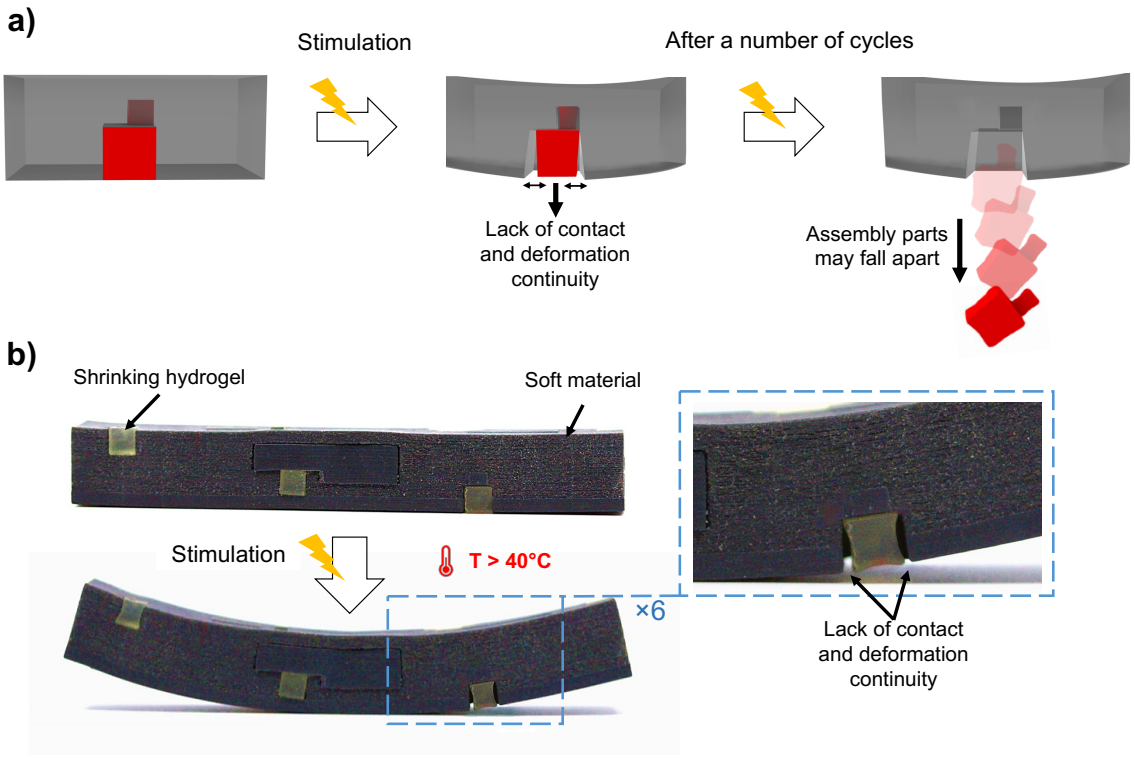

Figure 2. Current limitations of interlocking block assembly concerning the contact and deformation continuity: a) illustration scheme after multiple cycles of stimulation of a composite structure to achieve a bending, b) case of a shrinking hydrogel demonstrating the non-uniform overall deformation of the structure when thermally stimulated.

For instance, as illustrated in **Figure 2b**, even though the assembly remains stable after the stimulation, the external interfaces surrounding the shrinking hydrogel may not adhere properly. The shrinking hydrogel block fails to drive the neighboring interfaces, resulting in non-uniform or interrupted deformation in other terms. To overcome these challenges and generalize the applicability of the computational design approach, we will rely on the customization of interlocking blocks.

Therefore, the main idea of this paper is to customize the shapes of the interlocking blocks during the early stages of assembly generation, considering the specific SMs at our disposal and their potential transformations (isotropic or anisotropic behavior). By tailoring the block shapes to accommodate the behavior of the SMs, we aim to improve the uniformity of shape/property changes within the 4D multi-material interlocking assembly. Additionally, the limitations associated with the interfaces between blocks will be addressed, ensuring both contact continuity and deformation continuity which are two critical factors in achieving successful 4D printed structures. To assess the effectiveness of utilizing customized interlocking blocks, the physical behavior, and the stability of two assemblies will be compared (**Figure 3b and c**). Assembly B is derived from the previous interlocking assembly approach developed in [6-7], and Assembly C is generated using the customized interlocking blocks.

The structure of this paper will be organized as follows. The subsequent sections will initially describe the materials and methods involved in this study. Following that, comprehensive results and discussions will be presented, incorporating mechanical test results, simulations, and stimulations performed on illustrative cases. Lastly, the paper will conclude with a concise summary and closing remarks.

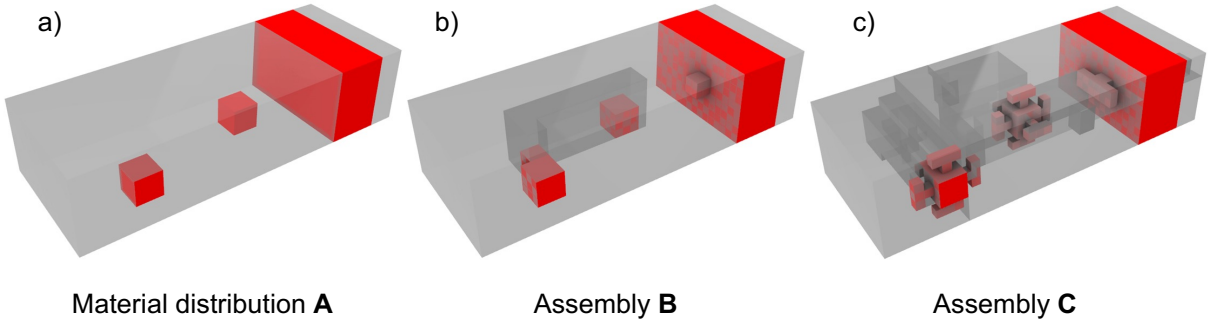

Figure 3. Illustrative case studies. Starting from (A) as the initial digital material distribution, (B) is the interlocking assembly generated from the previous interlocking approach developed in [6-7] (without customized interlocking blocks), and (C) is the interlocking assembly generated using customized interlocking blocks.

2. Materials and Methods

2.1. Materials

Two materials were used in this study. Agilus30™ was used as the inert material. The Agilus30™ is a soft and rubber-like material with a T_g of –10°C. Its liquid resin contains a photoinitiator, exo-1,7,7-trimethylbicyclo(2.2.1)hept-2-yl acrylate, urethane acrylate oligomer, methacrylate oligomer, and polyurethane resin [28]. A thermo-sensitive hydrogel was developed as the active material [29,30]. The formulation is prepared by mixing the N-isopropylacrylamide (NIPAM) monomers (50 wt% relative to the formulation) with PEG700-diacrylate crosslinker (2.5 wt% relative to the formulation) in ethylene glycol (50 wt%) as a non-reactive diluent. Irgacure TPO (3 wt% relative to the NIPAM and crosslinker) was added as the photoinitiator. All the chemical compounds were purchased from Sigma Aldrich (France).

2.2. Printing Parameters

The Agilus30™ parts were printed using a PolyJet™ Objet260 Connex3 printer (Stratasys®, Ltd., USA). This machine combines Inkjet technology and the use of photopolymers. A digital material mode at a resolution of 600 dpi along the *x*- and *y*-directions and a layer thickness of 30 µm and up to 85 µm for the *x*- and *y*-axes has been defined. The resins are polymerized by ultraviolet light with a spectral range of 300–450 nm. The hydrogel parts were printed using a digital light processing (DLP) 3D printer (Max X43, Asiga, Australia). The parts were constructed by photocrosslinking successive 100 µm thick resin layers. Each layer was irradiated at an intensity of 2.5 mW/cm² for 3 seconds. After printing, the hydrogel parts were first washed in ethanol and then several times with distilled water for 3 days.

2.3. Interlocking Assembly Generation Approaches

To thoroughly evaluate the efficiency of incorporating customized interlocking blocks based on SMs behavior, our investigation focuses on comparing the behavior and the stability of two distinct assemblies. The first assembly (labeled as Assembly B in Figure 3) is derived from the previously established interlocking assembly approach [6,7]. This approach served as the foundation for constructing an interlocking assembly without the utilization of a customized interlocking blocks. In contrast, the second assembly (labeled as Assembly C in Figure 3) will be generated using customized interlocking blocks. By conducting a detailed analysis of both assemblies, we aim to evaluate and compare their actuation performance and assembly stability.

2.3.1. Interlocking Assembly Generation Without Customized Interlocking Blocks

To generate Assembly B, the conventional approach is employed. Initially, a 3D/4D structure is established through machine learning or genetic algorithms, with a digital multi-material distribution (**Figure 4a**). This computational design approach, facilitated by the Rhinoceros3D/Grasshopper® software and the in-house VoxSmart add-on, determines homogeneous interlocking blocks of voxels. These blocks are designed to be printed separately using various AM techniques and materials, followed and subsequently assembly. This computational procedure is applied to an 80 x 18 x 30 mm^3 strip sample comprising 5,400 voxels, with each voxel having a volume of 2 mm^3.

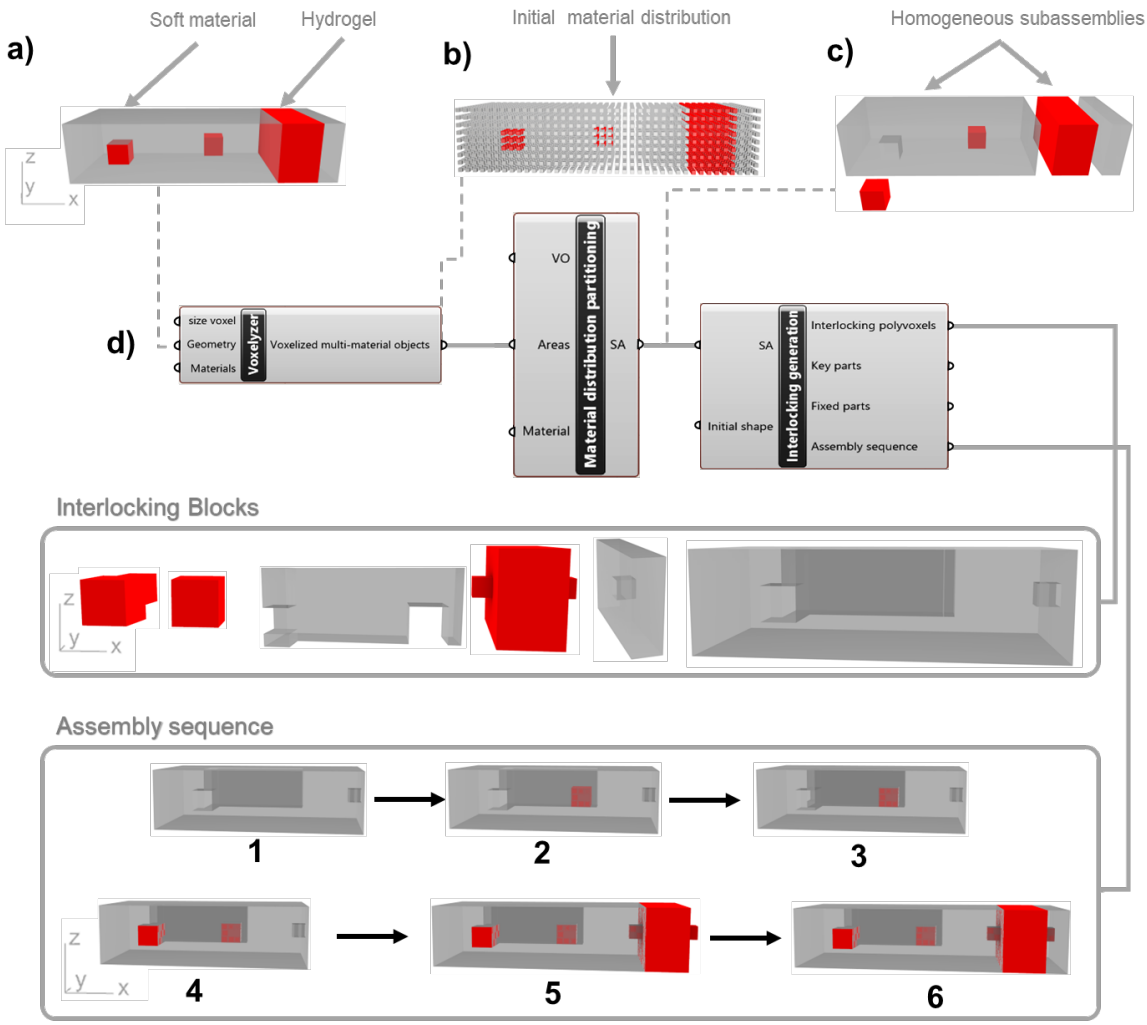

Figure 4. Computational design within Rhinoceros3D/Grasshopper® environment to determine the interlocking block assembly of an 80 x 30 x 18 mm^3 multi-material sample: (a) initial geometric structure highlighting the distribution of active/inert materials, (b) voxelization of the materials distribution, (c) homogeneous subassemblies after material distribution partitioning, (d) design program flow dedicated to the interlocking computation.

The process involves the three usual components: (i) the 'Voxelyzer' component, which obtains a voxel-based representation of the material distribution within the 3D/4D structure (**Figure 4b**), (ii) the 'Material distribution partitioning' component, which divides the structure into homogeneous parts based on material composition (**Figure 4c**), and (iii) the 'Interlocking generation' component, which generates interlocking blocks and determines the appropriate assembly sequence. These components are illustrated in **Figure 4d**.

2.3.2. Interlocking Assembly Generation with Customized Interlocking Blocks

The primary goal of this paper is to generate a 4D multi-material interlocking assembly after the customization of the interlocking blocks during the initial stages of the assembly computation. A crucial consideration in this process is understanding the potential transformations of specific SMs, whether they exhibit isotropic or anisotropic behavior. By incorporating this knowledge, the shapes of the

interlocking blocks can be optimized to align with the anticipated deformations. For instance, the behavior of hydrogels and liquid crystal elastomers (LCEs) can be compared. Hydrogels are known for their remarkable ability to absorb and retain water, resulting in significant swelling. When subjected to external stimuli, such as changes in temperature or pH, hydrogels can undergo isotropic swelling or shrinking in all directions due to their homogeneous network structure [30-31]. On the other hand, LCEs exhibit anisotropic behavior. LCEs are a class of soft materials that combine both the long-range orientational order of liquid crystals and the mechanical flexibility of elastomers. The anisotropic behavior of LCEs arises from the alignment of their liquid crystal domains, leading to a directional-dependent behavior when subjected to external stimuli, i.e., a reconfiguration of the material's properties along specific directions [30,32-35].

By introducing interlocking blocks' designs with T-shape designs aligned with the expected deformation direction (**Figure 5**), we intend to ensure both contact continuity and deformation uniformity at the block assembly interfaces. The T-shapes are added according to the digital material distribution, the isotropic/anisotropic behavior, and the location of the SM in a structure. Figure 5 hereafter gathers components that were developed in Rhinoceros3D/Grasshopper® using C# language to add T-shapes to the interlocking blocks considering the aforementioned points.

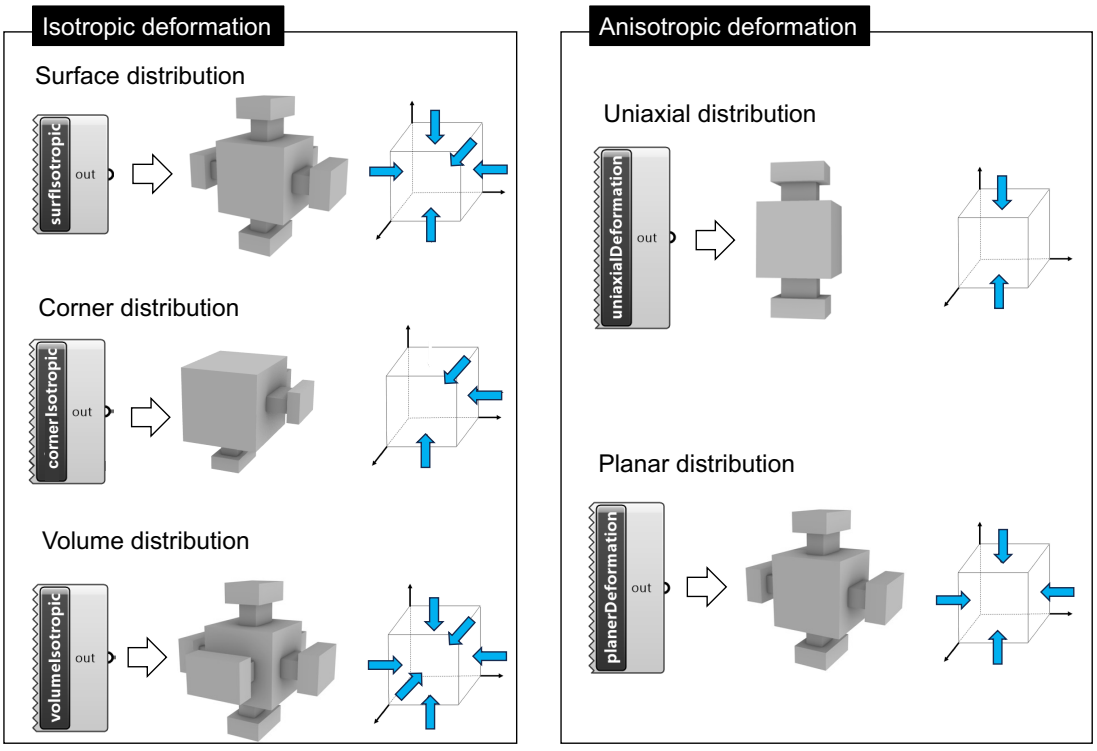

Figure 5. Customized T-shape interlocking blocks according to isotropic/anisotropic behavior and the location of SMs in the active composite structure.

After incorporating T-shapes based on the digital material distribution, the behavior (isotropic or anisotropic), and the location of the SMs within the structure, additional interlocking blocks will be generated to ease the overall assembly of the customized one. The interlocking assembly conditions

involved in the development of the algorithm remain consistent with those discussed in the first approach presented in [6,7]:

1- Only one translation direction is permitted for inserting each part into the assembly.
2- Each inserted part in the assembly effectively blocks the entire group of previously inserted parts, continuing until the key part(s) is ultimately inserted to secure the entire assembly.
3- Disassembly follows a single translation direction, with the key part(s) being the first to be disassembled.
4- Key parts are the only components that possess mobility within the assembly.

2.4. Assembly Stability

To compare the structural integrity and the assembly stability of both assemblies, namely Assembly B and Assembly C, a shaking test was performed. Also known as a vibration test, this destructive testing method is employed to assess the stability and performance of components under simulated dynamic conditions. The purpose of the test is to subject both assemblies to mechanical vibrations at a specific frequency to compare their ability to withstand vibrational environments. The vibrations can be applied in different directions and axes to cater to specific testing requirements. Test parameters such as amplitude and duration can be adjusted to simulate vibration scenarios or adhere to industry standards like DIN EN ISO 9000.

In our study, the RETSCH® Type 3D (RETSCH, Haan, Germany) machine vibrating mode was employed, with an amplitude of 70 mm (representing the vertical vibration height) and a frequency of 2600 vibrations per minute (vpm). During the shaking test, both assemblies were mounted on a vibration platform and subjected to three-dimensional movements, including circular motion combined with vertical throwing motion. As a result, the samples were uniformly dispersed throughout the entire vibration area while undergoing reorientations. The time taken for both assemblies to experience their first separation of interlocking parts was then measured. To ensure repeatability and consistency of the findings, five samples of each assembly underwent the shaking test using the same procedure.

2.5. Actuation Simulation

To assess and compare the physical behavior of both assemblies, a comprehensive analysis was conducted using simulation of physical deformations at multiple temperatures. This analysis was performed utilizing the in-house VoxSmart add-on simulator within the Rhinoceros3D/Grasshopper® environment [8,10,36]. The VoxSmart add-on also enables the generation of a computational predictive model of shape change in both assemblies when subjected to stimulation energy. The simulation temperatures were set at 25, 30, 35, 38, and 40 °C, then we extracted voxels' displacements from simulations.

2.6. Actuation Process

As mentioned in Section 2.1, hydrogel was incorporated as an active material in both multi-material assemblies B and C. In these assemblies, the PNIPAM hydrogel acts as an actuator, undergoing shrinkage when exposed to temperatures between 25 °C and 40 °C due to the gradual release of water initially absorbed. Thus, the hydrogel parts shrink, leading to an overall deformation of both assemblies. To assess the extent of contact continuity and make a comparison between the two assemblies, the samples were stimulated in hot water at 40 °C for a duration of 1 hour. Following the heating process, gap measurements were conducted from captured images of the samples to visually assess deformation and quantify the contact continuity. To ensure repeatability and reliability of the results, five samples of each assembly were tested using the same procedure.

It is worth noting that the samples can recover their initial shape when immersed in distilled water at room temperature (RT) for at least two days. This recovery process demonstrates the reversible behavior of the hydrogel actuation. **Figure 6** provides a visual representation of the actuation and recovery procedures involved in the testing process.

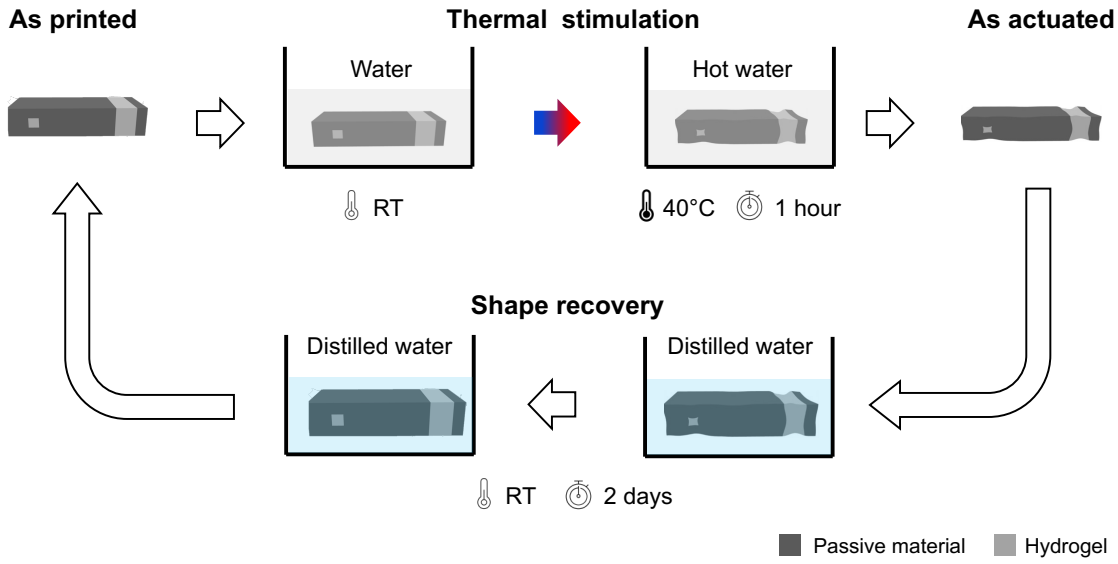

Figure 6. Actuation in hot water at 40°C and recovery procedures in distilled water at RT of the interlocking assembly case studies.

3. Results and Discussion

3.1. Interlocking Assembly Generation with Customized Interlocking Blocks

After customizing the interlocking shapes of the SMs based on the digital material distribution, the behavior (isotropic or anisotropic), and their location within the structure, the algorithm proceeds by voxelizing the remaining inert space that encapsulates the SMs using the 'voxelizer left space' component (**Figure 7a**). This component generates a list of points which, with the assistance of

mathematical models such as directed blocking graphs (DBGs) and adjacency matrices, as referred in [6,7], will be utilized to generate the interlocking assembly. To do so, another component, labeled as the 'Interlocking generator' is developed (**Figure 7b**). This component computes the interlocking block assembly and determines the suitable assembly sequence (**Figure 7c and d**).

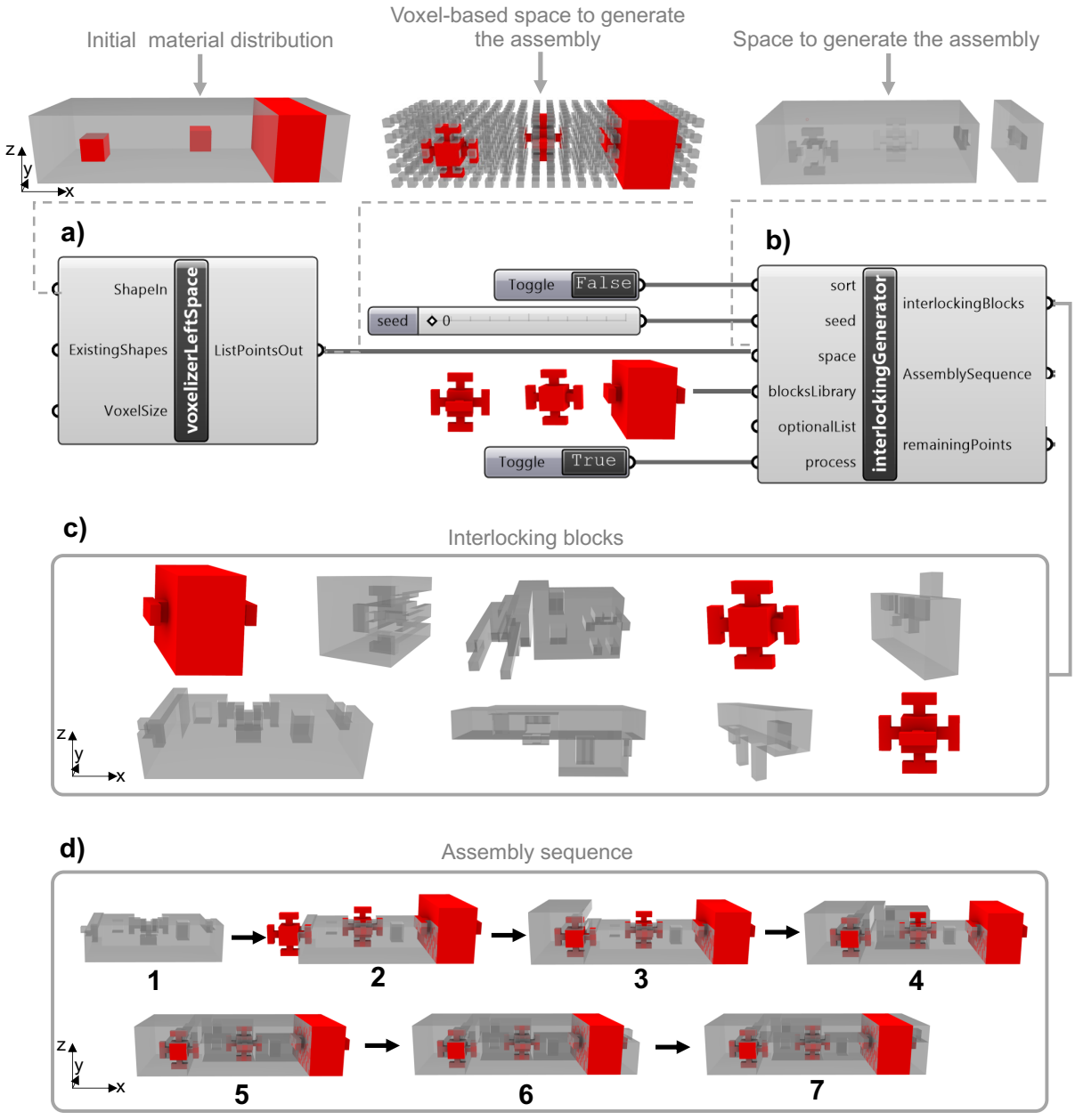

Figure 7. Computational design process flow within Rhinoceros3D/Grasshopper® to determine the interlocking block assembly of the 80 x 30 x 18 mm^3 multi-material sample, the red color refers to the hydrogel and the grey color to the inert material: (a) voxelization of the remaining space component's initial geometric structure, highlighting the distribution of active/inert materials, (b) the interlocking assembly generator component for (c) generating the interlocking blocks, and (d) the related assembly sequence.

The algorithm generates numerous interlocking assemblies with their assembly sequence (**Figure 8a**) based on the chosen seed (as shown through the red nodes in the graphs of **Figure 8b**),

which governs the selection of voxel candidates during the interlocking assembly computation. **Figure 8** provides one admissible interlocking assembly generated by the tool, accompanied by the corresponding DBGs and adjacency matrices.

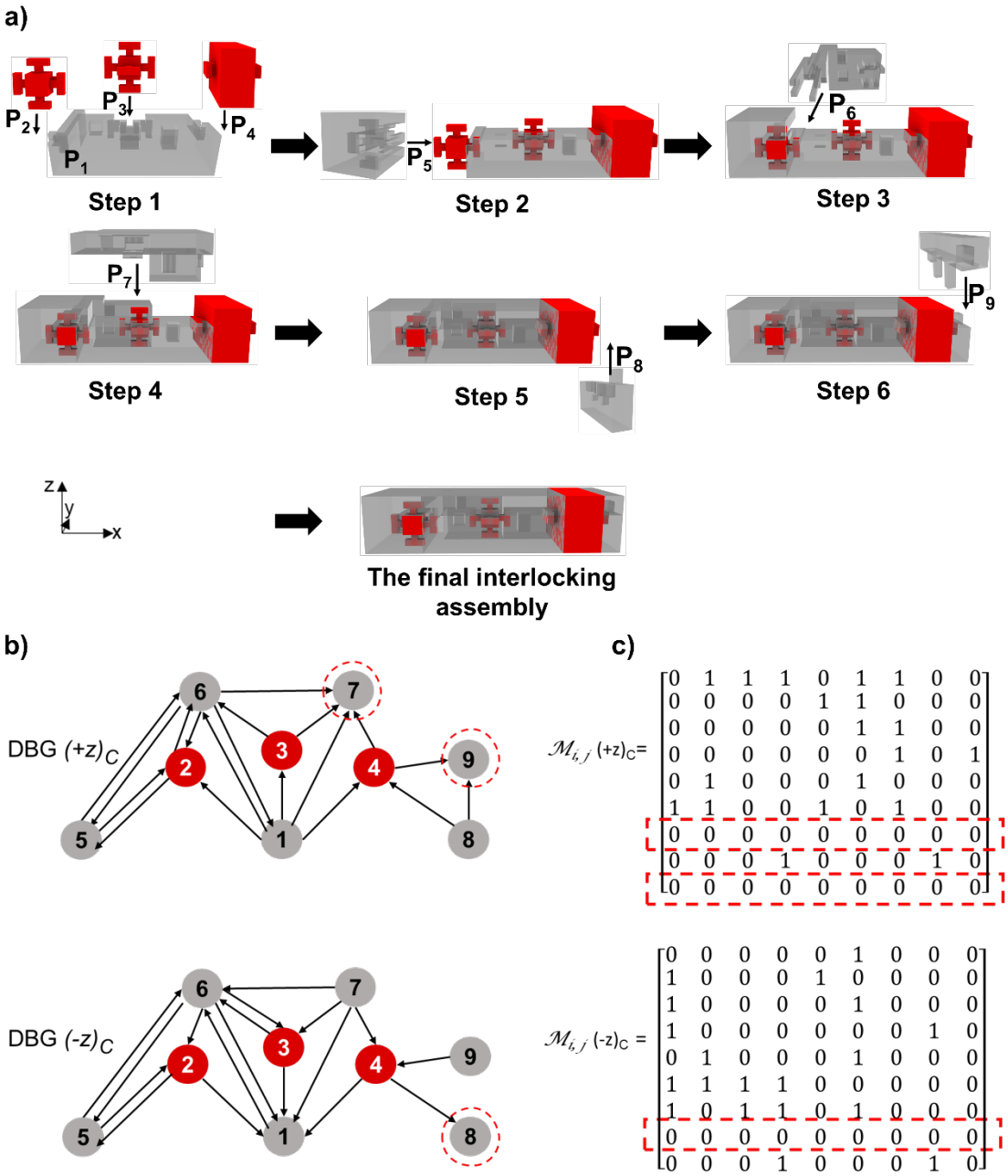

Figure 8. Multi-material interlocking assembly generated using customized interlocking blocks. (a) description of one of the admissible assembly sequence of the multi-material 4D printed sample, 6 blocks have been determined by the in-house VoxSmart tool in addition to the customized blocks, (b) the DGB of the final interlocking assembly, the nodes represent the 9 blocks of the assembly, an ordered pair (arrow) between P_1 and P_2 means that P_1 is blocked by P_2 along a direction d, the dashed red circles illustrate the key parts in the direction d, and (c) related adjacency matrices.

3.2. Assembly Stability

After physically printing the PNIPAM hydrogel and the Agilus30^{TM} interlocking blocks, Assembly B and Assembly C were manually constructed, as depicted in **Figure 9**. Subsequently, both assemblies were mounted onto the vibration platform.

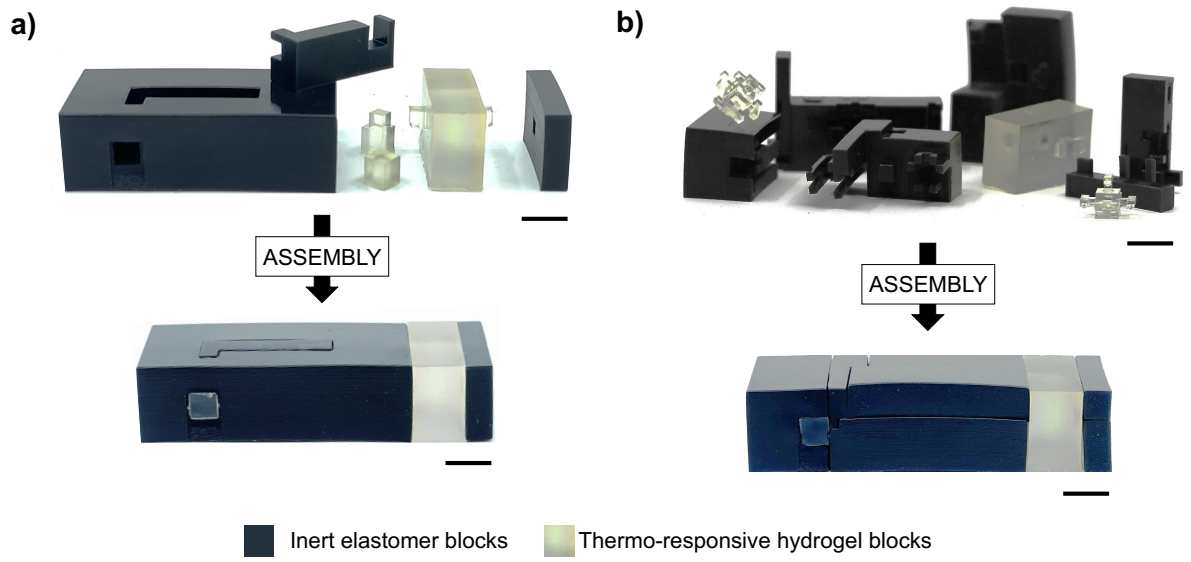

Figure 9. Printed interlocking blocks and related assemblies. (a) Assembly B and (b) Assembly C with customized T-shape interlocking parts. Transparent parts

A uniform amplitude of vibration, set at 70 mm, was applied to both assemblies until the initial disassembly of the interlocking parts occurred. The duration required for this disassembly event was carefully measured for each assembly, as displayed in the **Figure 10**. This experimental setup allowed for a comparative assessment of the stability and durability of the interlocking structures in Assembly B and Assembly C, shedding light on their respective performance under the applied vibrations.

The results obtained from the measurement of the time until the first break-up event in the assemblies revealed an interesting observation. Assembly B exhibited a relatively short period of 8 min before experiencing the first interlocking block separation. On the other hand, Assembly C, which had customized interlocking blocks, displayed a significantly longer duration of 48 min before encountering its initial block detachment. These results highlight the substantial impact that the customization of interlocking blocks with T-shapes can have on the stability of the overall assembly. By tailoring the interlocking blocks to suit the specific requirements and characteristics of the materials used, Assembly C demonstrated enhanced resistance to separation, ensuring a more robust and durable interlocking multi-material structure. These results validate the effectiveness of the proposed approach in improving the stability and integrity of interlocking assemblies.

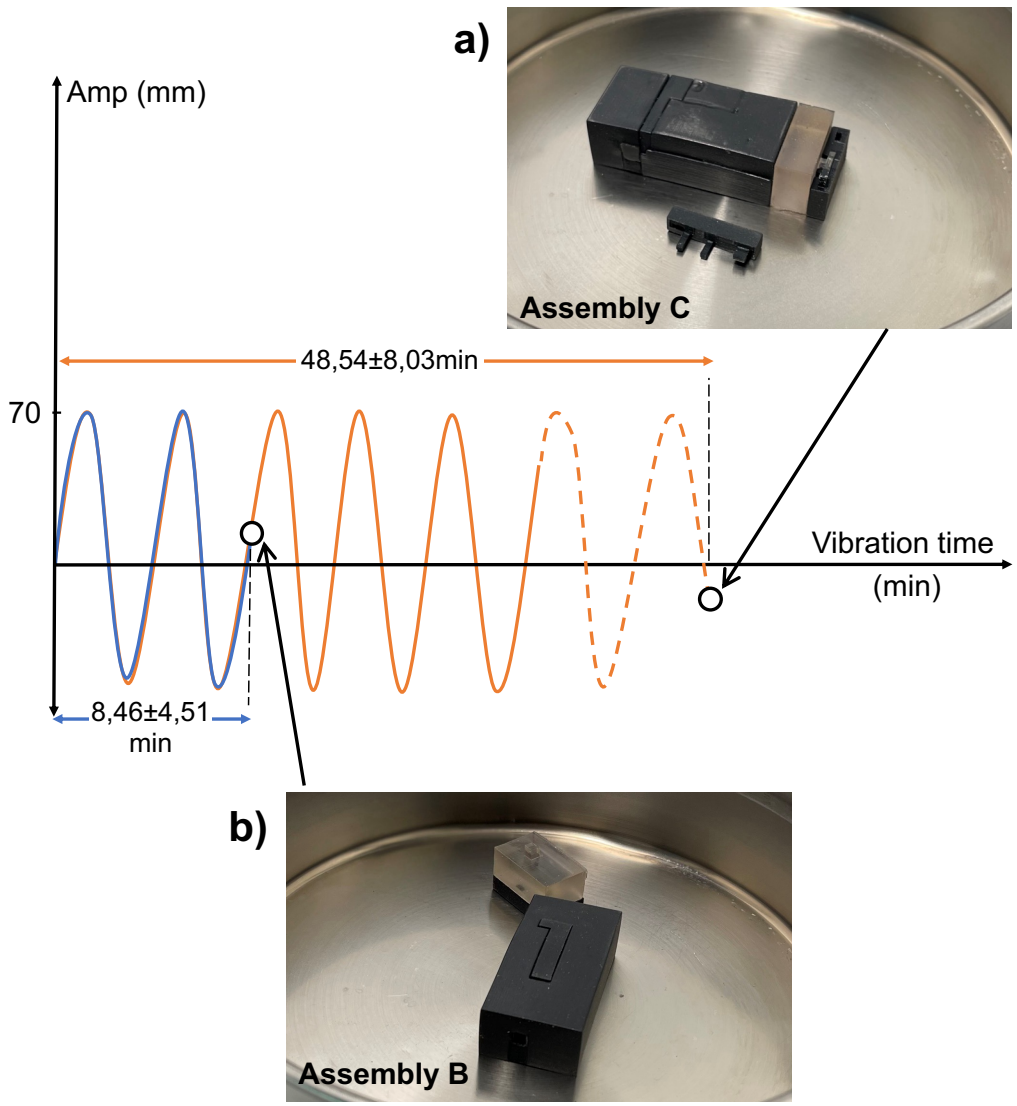

Figure 10. Shaking test results. The blue graph refers to the performance of Assembly B and the orange graph refers to the performance of Assembly C: (a) first Assembly C part separation and (b) first Assembly B part separation.

3.3. Actuation Simulation

Through simulation, the response of each assembly is evaluated under various temperature conditions using the in-house VoxSmart add-on simulator within the Rhinoceros3D/Grasshopper® environment (**Figure 11**). This allows for a thorough understanding and comparison of how temperature influences the structural integrity and deformation patterns of the two assemblies. Furthermore, voxels displacements along the X, Y, and Z axes in the two assemblies are obtained after a stimulation at 25, 30, 35, 38, and 40 °C. The computed displacements are then used to compare both Assembly B and Assembly C regarding their physical behavior in the presence of energy stimulation. To do so, vector moduli are measured, which represent the distance between the position of a voxel (v_B) in Assembly B and its position (v_C) in Assembly C. The vector moduli are given as follows (see Equation 1):

$$\| \overrightarrow{v_C v_B} \| = \sqrt{(U_{x_C} - U_{x_B})^2 + (U_{y_C} - U_{y_B})^2 + (U_{z_C} - U_{z_B})^2} \quad (1)$$

where $v_B = (U_{x_B}, U_{y_B}, U_{z_B})$ and $v_C = (U_{x_C}, U_{y_C}, U_{z_C})$ are displacements vectors of the voxels in Assembly B and Assembly C respectively.

Based on the results obtained from the simulations and distance calculations, **Figure 11** and **Table 1** provide evidence that the differences in deformation between the two structures are negligible. This holds true across various temperatures: 30 °C, 35 °C, 38 °C, and 40 °C. For example, in Table 1 that outlines the maximum and average distances between the positions of voxels in the two assemblies, the average distance between a voxel in Assembly B and its corresponding position in Assembly C at 40 °C is found to be 0.223 mm. This distance is relatively small compared to the overall length of the 80 mm sample. These findings indicate that the use of customized interlocking blocks for assembly generation does not compromise the shape-change properties of the 4D-printed structure. The implementation of the customized blocks has been successful in maintaining the physical properties of the assembly throughout its deformations from a simulation perspective.

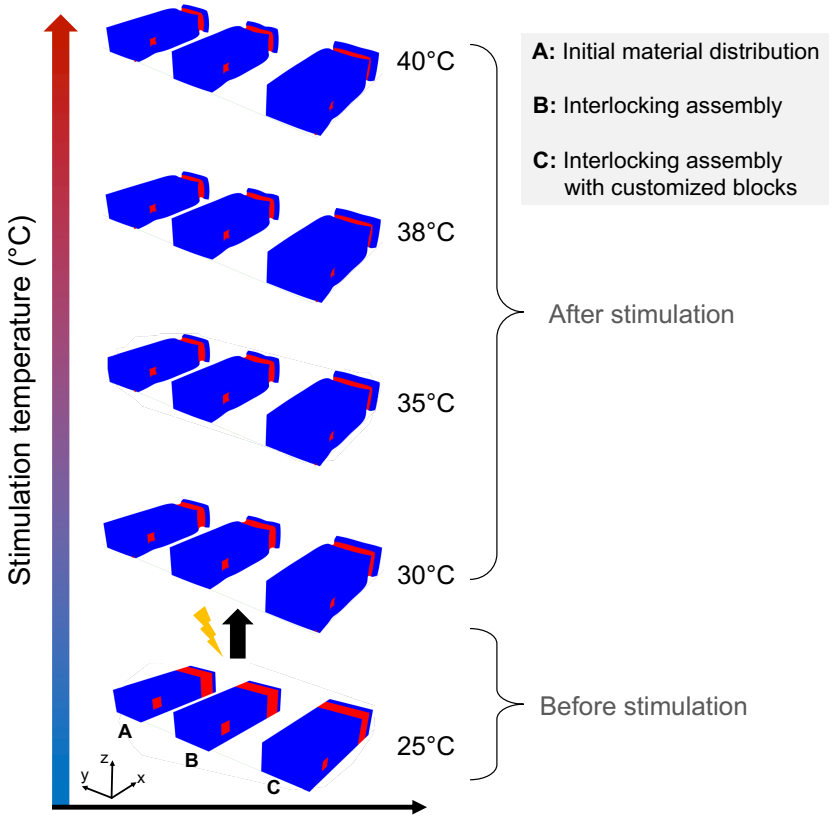

Figure 11. Simulation of multi-material 4D printed structures using the in-house VoxSmart add-on within the Rhinoceros3D/Grasshopper® environment. (A) initial distribution, (B) the interlocking assembly without using customized blocks, and (C) the interlocking assembly using customized blocks. Simulations were performed before stimulation at 25 °C and after stimulation at 30 °C, 35 °C, 38 °C, and 40 °C.

Table 1. Calculation of the maximum and average distances between positions of voxels in (B) the interlocking assembly without using customized blocks and (C) the interlocking assembly using customized blocks at 25 °C, 30 °C, 35 °C, 38 °C, and 40 °C.

Temperature (°C)	Maximum distance [mm ±0.01]	Average distance [mm ±0.01]
25	0	0
30	0.326	0.273
35	0.388	0.244
38	0.481	0.192
40	0.356	0.223

3.4. Actuation Process

To evaluate the level of contact continuity and facilitate a comparative analysis between the two assemblies, the following testing protocol was implemented. The samples were subjected to a controlled heating process in water at 40 °C for a duration of 1 hour. This thermal treatment aimed to induce deformation within the assemblies due to the presence of a thermo-sensitive hydrogel. After the heating process, high-resolution images of the samples were captured, and gap measurements were conducted using the ImageJ software tool (version 46r). The focus of the analysis was on the interfaces between the hydrogel blocks, indicated by the red arrows in **Figure 12**. It is important to note that due to time constraints, the investigation was limited to the interfaces of the appearing hydrogel blocks, and the internal volume interfaces were not examined.

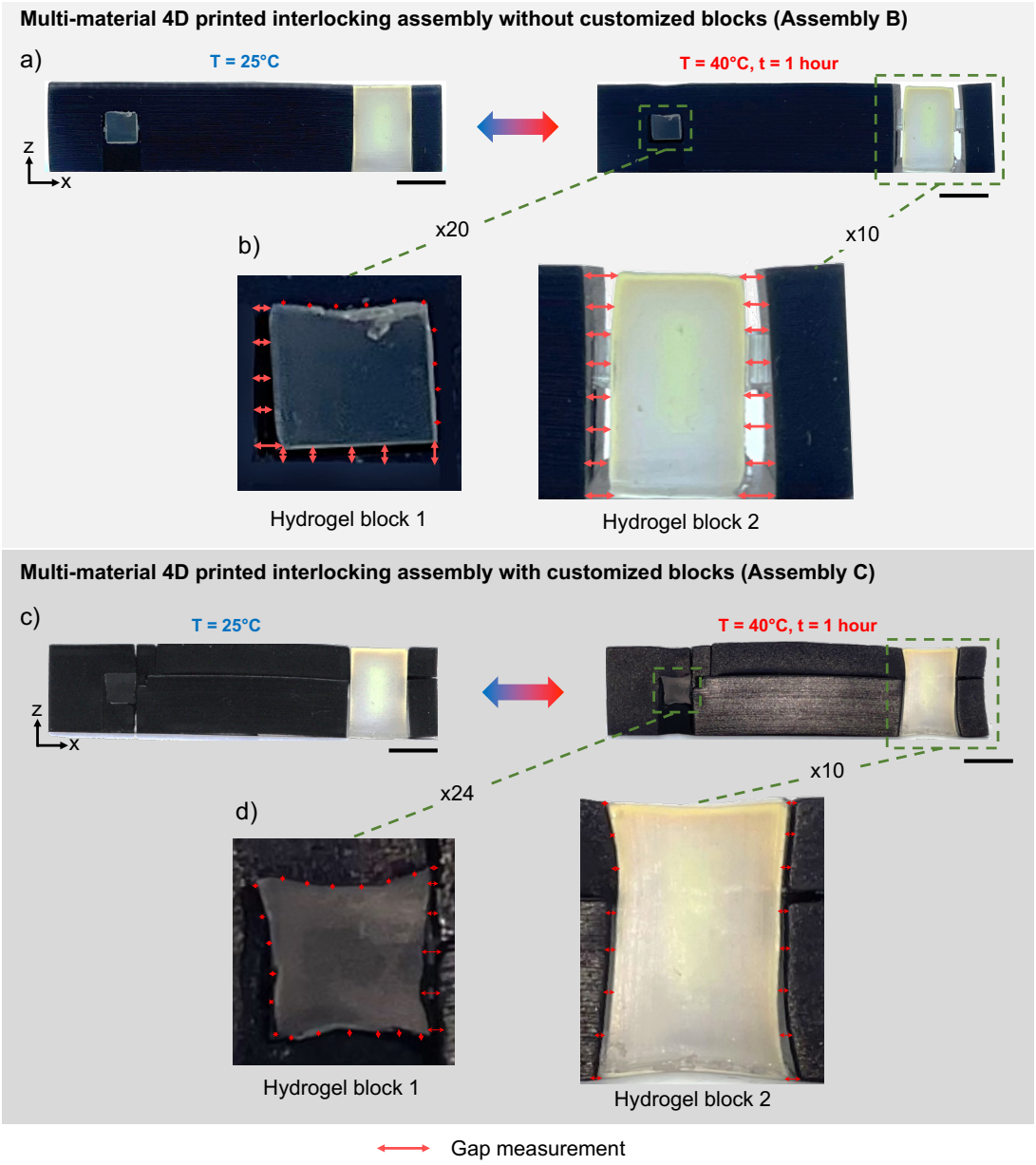

Figure 12. Multi-material 4D printed interlocking assembly without customized blocks (Assembly B): (a) manual assembly of the interlocking blocks following the assembly sequence generated by the developed VoxSmart component and related deformed structure after stimulation at 40 °C for 1 hour, (b) hydrogel block 1 deformation zooming in (Focus x20) and hydrogel block 2 deformation zooming in (Focus x10). Multi-material 4D printed interlocking assembly with customized blocks (Assembly C): (c) manual assembly of the interlocking blocks and deformed structure after stimulation at 40 °C for 1 hour, (d) hydrogel block 1 deformation zooming in (Focus x24) and hydrogel block 2 deformation zooming in (Focus x10). Scale bars: 10 mm.

A total of five samples from each assembly were tested using the same procedure to ensure repeatability and reliability of the results. The measured gap data were compiled and presented in **Figure 13**, providing valuable insights into the contact continuity between the hydrogel and inert materials within the interlocking assemblies. In terms of contact and deformation continuity, the analysis presented in Figure 11 demonstrates the superior performance of Assembly C, which incorporates customized interlocking blocks, compared to Assembly B (interlocking assembly without customized

blocks). For instance, the measured gaps at the interfaces of hydrogel block 1 in Assembly C are significantly smaller, with a measurement of 0.05 mm, in contrast to Assembly B where the measurement reaches 0.55 mm (approximately 10 times larger). This observation holds true in the gap measurements at the interfaces of hydrogel block 2. The introduction of T-shapes to the hydrogel blocks, based on their deformations, has played a crucial role in enabling the neighboring blocks to adapt to the deformations of the hydrogel material. This implementation has resulted in improved assembly stability and enhanced contact continuity within the interlocking assembly.

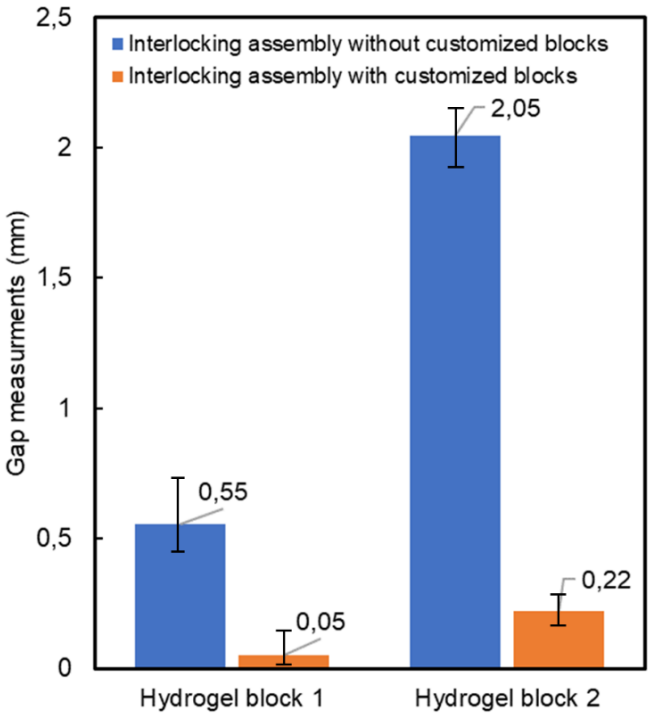

Figure 13. Gap measurements at hydrogel blocks 1 and 2 interfaces. Blue color refers to Assembly B while the orange color refers to Assembly C.

While it is evident that the customized blocks contributed to improved contact continuity and deformation, it is important to investigate other smart materials to further demonstrate the generalization and the applicability of the proposed approach. Further research and experimentation with such materials will add value and strengthen the potential of the interlocking assembly with customized blocks.

4. Conclusion

In conclusion, the main objective of this paper was to introduce a customization approach for the shapes of interlocking blocks during the initial stages of assembly generation. This approach takes into consideration properties of SMs and their potential transformations, whether they exhibit isotropic or anisotropic behavior. The aim is to optimize the interlocking block shapes to accommodate the behavior of the SMs, thereby enhancing the uniformity of shape and property changes within the 4D multi-material interlocked assembly. By customizing the interlocking block shapes, the limitations associated

with the interfaces between blocks are addressed, focusing on two critical factors: contact continuity and deformation continuity. Ensuring seamless contact between blocks is essential for maintaining the structural integrity and stability of the interlocked assembly. Simultaneously, achieving smooth deformation transitions between blocks is crucial for achieving the desired shape-changing properties of the 4D printed structures. To evaluate the effectiveness of utilizing customized interlocking blocks, the physical behavior and stability of two assemblies were compared: one based on the previous interlocking assembly approach developed in [6,7], which did not employ customized blocks, and the other generated using the customized interlocking blocks.

Through experimental testing and analysis, we observed notable improvements in both contact continuity and deformation continuity in the assembly utilizing the customized interlocking blocks (Assembly C) compared to the assembly without customized blocks (Assembly B). The customized block design, tailored to the specific behavior of the SMs, facilitated better contact between blocks and enhanced the overall stability of the assembly. Future work will explore, test, and improve this approach by considering other SMs and metamaterials [37,38] with greater mechanical properties to fully harness the potential of this approach and achieve optimal deformation in practice.

Acknowledgements

This work was supported by the IUF, a French government grant managed by the French Research Agency (ANR) under the “France 2030” initiative and the DIADEM program (ANR-22-PEXD-0013, “ARTEMIS”), the EIPHI Graduate School (Contract ANR-17-EURE-0002), and Bourgogne Franche-Comté Region.

References

[1] F. Heibeck, B. Tome, C. Della, S. Hiroshi. uniMorph - fabricating thin-film composites for shape-changing interfaces. In UIST ’15 Proceedings of the 28th Annual ACM Symposium on User Interface Software & Technology, 2015.

[2] Z. Ding, C. Yuan, X. Peng, T. Wang, H.J. Qi, M.L. Dunn. Direct 4D printing via active composite materials. Science advances 2017, 3(4), e1602890.

[3] F. Demoly, M.L. Dunn, K.L. Wood, H.J. Qi, J.C. André. The status, barriers, challenges, and future in design for 4D printing. Materials & Design 2021, 212, 110193.

[4] A. Haleem, M. Javaid, R. P. Singh, R. Suman. Significant roles of 4D printing using smart materials in the field of manufacturing. Adv. Ind. Eng. Polym. Res. 2021, 4(4), 301-311.

[5] F. Demoly, J.C. André. Impression 4D : promesses ou futur opérationnel ? Techniques de. l’Ingénieur 2021, RE285. https://doi.org/10.51257/a-v1-re285

[6] K. Benyahia, H. Seriket, R. Prod’hon, S. Gomes, J.C. André, H.J. Qi, F. Demoly. A computational design approach for multi-material 4D printing based on interlocking blocks assembly. Additive Manufacturing 2022, 58, 102993.

[7] K. Benyahia, S. Gomes, J.C. André, H.J. Qi, F. Demoly. Influence of interlocking blocks assembly on the actuation time, shape change, and reversibility of voxel-based multi-material 4D structures. Smart Materials and Structures 2023, 32(6), 065011.

[8] G. Sossou, F. Demoly, H. Belkebir, H.J. Qi, S. Gomes, G. Montavon. Design for 4D printing: A voxel-based modeling and simulation of smart materials. Materials & Design 2019, 175, 107798.

[9] C.M. Hamel, D.J. Roach, K.L. Long, F. Demoly, M.L. Dunn, H.J. Qi. Machine-learning based design of active composite structures for 4D printing. Smart Materials and Structures 2029, 28(6), 065005.

[10] G. Sossou, F. Demoly, H. Belkebir, H.J. Qi, S. Gomes, G. Montavon. Design for 4D printing: Modeling and computation of smart materials distributions. Materials & Design 2019, 181, 108074.

[11] F. Demoly, J.C. André. 4D Printing, Volume 1: Between disruptive research and industrial applications. ISTE-Wiley, London, UK, 368p., 2022.

[12] F. Demoly, J.C. André. 4D Printing, Volume 2: Between science and engineering". ISTE-Wiley, London, UK, 320p., 2022.

[13] F. Demoly, J.C. André, Research strategy in 4D printing: Disruptive vs incremental? Journal of Integrated Design and Process Science 2020, 24, 53-73, https://doi.org/10.3233/JID200020.

[14] A. Costa, A. Abdel-Rahman, J. Benjamin, N. Gershenfeld, I. Kostitsyna, K. Cheung. Algorithmic Approaches to Reconfigurable Assembly Systems. IEEE Aerospace Conference Proceedings 2019.

[15] M. Delmans, J. Haseloff. μCube: A Framework for 3D Printable Optomechanics. Journal of Open Hardware 2018, 2(1).

[16] D. Wang, M. Hermes, R. Kotni, Y.Wu, N. Tasios, Y. Liu, B. de Nijs, E.B. van der Wee, C.B. Murray, M. Dijkstra, A. van Blaaderen. Interplay between Spherical Confinement and Particle Shape on the Self-Assembly of Rounded Cubes. Nature Communications 2018, 9, 2228.

[17] L. Aaron, N. Michelson, B. Minevich, Y. Fleger, M. Stern, A. Shaulov, Y. Yeshurun, O. Gang 2020. DNA-Assembled Superconducting 3D Nanoscale Architectures. Nature Communications 2020, 11, 5697.

[18] L. Yuan, S. Zhuo, Y. Xiao, G. Zheng, G. Dong, F. Z. Yaoyao. Rapid Modeling and Design Optimization of Multi-Topology Lattice Structure Based on Unit-Cell Library. Journal of Mechanical Design 2020, 142(9), 091705.

[19] J. Benjamin, N. Gershenfeld, M. Carney, S. Calisch, W. Spencer. Digital Morphing Wing: Active Wing Shaping Concept Using Composite Lattice-Based Cellular Structures. Soft Robotics 2017, 4(1), 33-48.

[20] S.G. Shih, The art and mathematics of self-interlocking SL blocks, Bridges Conference Proceedings, Tesselations Publishing (2018) 107-114.

[21] Shih, S. G. Grammars of Interlocking SL Blocks. Bridges 2020 Conference Proceedings.

[22] Shih, S. (2016). Advances in Architectural Geometry 2016, Chapter On the Hierarchical Construction of SL Blocks – A Generative System that Builds Self-Interlocking structures. Hochschulverlag AG an der ETH Zürich.

[23] C. Fu, X. Yan, L. Yang, P. Jayaraman, D. Cohen-Or. Computational interlocking furniture assembly. Journal of ACM Transactions on Graphics (TOG), Proceeding of ACM SIGGRAPH 2015.

[24] A. Kanel-Belov, A. Dyskin, Y. Estrin, E. Pasternak, I. Ivanov-Pogodaev. Interlocking of convex polyhedra: towards a geometric theory of fragmented solids. Moscow Mathematical Journal 2010, 10(2), 337–342.

[25] K.Y. Lo, C.W. Fu, H. Li. 3d polyomino puzzle. ACM Trans. Graph. 2009, 28(5), 1-8.

[26] M. Weizmann, O. Amir, Y.J. Grobman. Topological interlocking in architecture: A new design method and computational tool for designing building floors. International Journal of Architectural Computing 2017, 15(2), 107-118.

[27] H. Yong. Utilisation of topologically-interlocking osteomorphic blocks for multi-purpose civil construction. Ph.D. Dissertation, University of Western Australia, Australia, 2011.

[28] Stratasys. Agilus30 Material Datasheet. https://support.stratasys.com/en/materials/material-datasheets/agilus30/.

[29] M.A. Haq, Y. Su, D. Wang. Mechanical properties of PNIPAM based hydrogels: A review. Materials Science and Engineering: C, 2017, 70, 842-855.

[30] W.J. Zheng, N. An, J.H. Yang, J. Zhou, Y.M. Chen. Tough Al-alginate/poly (N-isopropylacrylamide) hydrogel with tunable LCST for soft robotics. ACS applied materials & interfaces 2015, 7(3), 1758-1764.

[31] A. Sydney Gladman, Matsumoto A., Nuzzo R.G., Mahadevan L., Lewis J.A. Biomimetic 4D printing. Nature Materials 2016, 15, 413-418.

[32] D.J. Roach, C. Yuan, X. Kuang, V.C.F. Li, P. Blake, M.L. Romero, Hammel I., K. Yu, H.J. Qi. Long liquid crystal elastomer fibers with large reversible actuation strains for smart textiles and artificial muscles. ACS applied materials & interfaces 2019, 11(21), 19514-19521.

[33] M. Chen, Y. Hou, R. An, H.J. Qi, K. Zhou. 4D printing of reprogrammable liquid crystal elastomers with synergistic photochromism and photo-actuation. Advanced Materials 2023, 2303969.

[34] S. Leanza, S. Wu, X. Sun, H.J. Qi, R.R. Zhao. Active Materials for Functional Origami. Advanced Materials 2023, 2302066.

[35] X. Peng, S. Wu, X. Sun, L. Yue, S.M. Montgomery, F. Demoly, K. Zhou, R.R. Zhao, H.J. Qi. 4D printing of freestanding liquid crystal elastomers via hybrid additive manufacturing. Advanced Materials 2022, 34(39), 2204890.

[36] G. Sossou, H. Belkebir, F. Demoly. Multimaterial 4D printing simulation using a grasshopper plugin. In Smart Materials in Additive Manufacturing, Vol. 2: 4D Printing Mechanics, Modeling, and Advanced Engineering Applications (Eds: M. Bodaghi, A. Zolfagharian), Elsevier, 329-345.

[37] T. Li, J. Li, X. Huang, Experimental investigation on 4D printed intelligent assembly cushion with adjustable pre-tightening force. Smart Materials and Structures 2023, 32, 105001.

[38] M. Sun, K. Zhang, X. Guo, Z. Zhang, Y. Chen, G. Zhang, S. Jiang. A novel negative stiffness metamaterials: discrete assembly and enhanced design capabilities. Smart Materials and Structures 2023, 32, 095036.